

# ZrO<sub>2</sub>-TiO<sub>2</sub> thin films: a new material system for mid-infrared integrated photonics

Ningyuan Duan,<sup>1</sup> Hongtao Lin,<sup>2</sup> Lan Li,<sup>2</sup> Juejun Hu,<sup>2</sup> Lei Bi,<sup>1\*</sup> Haipeng Lu,<sup>1</sup> Xiaolong Weng,<sup>1</sup> Jianliang Xie<sup>1</sup> and Longjiang Deng<sup>1</sup>

<sup>1</sup>State Key Laboratory of Electronic Thin Films and Integrated Devices, University of Electronic Science and Technology of China, Chengdu 610054, China

<sup>2</sup>Department of Materials Science & Engineering, University of Delaware, Newark, Delaware, 19716, USA  
[\\*bilei@uestc.edu.cn](mailto:bilei@uestc.edu.cn)

**Abstract:** Mid-infrared (MIR, 2 - 6  $\mu\text{m}$  wavelength) transparent metal oxides are attractive materials for planar integrated MIR photonic devices and sensing applications. In this report, we present reactive sputtering deposited ZrO<sub>2</sub>-TiO<sub>2</sub> (ZTO) thin films as a new material candidate for integrated MIR photonics. The material structure and optical properties were systematically studied as a function of Ti concentration. The thin film index of refraction monotonically increases with Ti concentration, while the film crystallinity decreases. Fully amorphous ZTO films were achieved with 40 at.% Ti doping on various substrates. MIR micro-disk resonators on MgO substrates were demonstrated using Zr<sub>0.6</sub>Ti<sub>0.4</sub>O<sub>2</sub> strip-loaded waveguides with a loaded quality factor of  $\sim 11,000$  at 5.2  $\mu\text{m}$  wavelength.

©2013 Optical Society of America

**OCIS codes:** (160.2750) Glass and other amorphous materials; (310.3840) Materials and process characterization; (240.0310) Thin films; (140.4780) Optical resonators

---

## References and links

1. F. Leo, B. Kuyken, N. Hattasan, R. Baets, and G. Roelkens, "Passive SOI devices for the short-wave infrared," 16th European Conference on Integrated Optics (ECIO 2012), Spain, p. 156 (2012)
2. Y. Xia, C. Qiu, X. Zhang, W. Gao, J. Shu, and Q. Xu, "Suspended Si ring resonator for mid-IR application," *Opt. Lett.* **38**(7), 1122–1124 (2013).
3. C. Y. Wong, Z. Cheng, X. Chen, K. Xu, C. K. Y. Fung, Y. Chen, and H. K. Tsang, "Characterization of Mid-Infrared Silicon-on-sapphire Microring Resonators With Thermal Tuning," *J. IEEE Photonics* **4**(4), 1095–1102 (2012).
4. A. Spott, Y. Liu, T. Baehr-Jones, and M. Hochberg, "Silicon waveguides and ring resonators at 5.5  $\mu\text{m}$ ," *Appl. Phys. Lett.* **97**(21), 213501 (2010).
5. R. Shankar, I. Bulu, and M. Loncar, "Integrated high-quality factor silicon-on-sapphire ring resonators for the mid-infrared," *Appl. Phys. Lett.* **102**(5), 051108 (2013).
6. H. Lin, L. Li, Y. Zou, S. Danto, J. D. Musgraves, K. Richardson, S. Kozacik, M. Murakowski, D. Prather, P. T. Lin, V. Singh, A. Agarwal, L. C. Kimerling, and J. Hu, "Demonstration of high-Q mid-infrared chalcogenide glass-on-silicon resonators," *Opt. Lett.* **38**(9), 1470–1472 (2013).
7. R. Shankar, R. Leijssen, I. Bulu, and M. Loncar, "Mid-infrared photonic crystal cavities in silicon," *Opt. Express* **19**(6), 5579–5586 (2011).
8. H. Lin, L. Li, F. Deng, C. Ni, S. Danto, J. D. Musgraves, K. Richardson, and J. Hu, "Demonstration of mid-infrared waveguide photonic crystal cavities," *Opt. Lett.* **38**(15), 2779–2782 (2013).
9. J. D. B. Bradley, C. C. Evans, F. Parsy, K. C. Phillips, R. Senaratne, E. Marti, and E. Mazur, "Low-loss TiO<sub>2</sub> planar waveguides for nanophotonic applications," in *IEEE Photonics Society 2010 23rd Annual Meeting*, (IEEE, 2011), pp. 313–314.
10. G. You, W. Guo, C. Zhang, P. Bhattacharya, and J. Xu, "Excitation dependent two-component spontaneous emission and ultrafast amplified spontaneous emission in dislocation-free InGaN nanowires," *Appl. Phys. Lett.* **102**, 091105 (2012).
11. R. Schermer, W. Berglund, C. Ford, R. Ramberg, and A. Gopinath, "Optical amplification at 1534 nm in erbium-doped zirconia waveguides," *IEEE J. Quantum Electron.* **39**(1), 154–159 (2003).
12. J. T. Choy, J. D. B. Bradley, P. B. Deotare, I. B. Burgess, C. C. Evans, E. Mazur, and M. Loncar, "Integrated TiO<sub>2</sub> resonators for visible photonics," *Opt. Lett.* **37**(4), 539–541 (2012).
13. "Nonlinear Optical Materials," in *Encyclopedia of Materials: Science and Technology*, Robert W. Boyd and George L. Fischer, eds. (2001).

14. D. L. Wood and K. Nassau, "Refractive index of cubic zirconia stabilized with yttria," *Appl. Opt.* **21**(16), 2978–2981 (1982).
15. T. J. Kippenberg, R. Holzwarth, and S. A. Diddams, "Microresonator-based optical frequency combs," *Science* **332**(6029), 555–559 (2011).
16. J. Kischkat, S. Peters, B. Gruska, M. Semtsiv, M. Chashnikova, M. Klinkmüller, O. Fedosenko, S. Machulik, A. Aleksandrova, G. Monastyrskyi, Y. Flores, and W. T. Masselink, "Mid-infrared optical properties of thin films of aluminum oxide, titanium dioxide, silicon dioxide, aluminum nitride, and silicon nitride," *Appl. Opt.* **51**(28), 6789–6798 (2012).
17. D. C. Cronemeyer, "Electrical and optical properties of rutile single crystals," *Phys. Rev.* **87**(5), 876–886 (1952).
18. J. Hu, V. Tarasov, N. Carlie, N. N. Feng, L. Petit, A. Agarwal, K. Richardson, and L. C. Kimerling, "Si-CMOS-compatible lift-off fabrication of low-loss planar chalcogenide waveguides," *Opt. Express* **15**(19), 11798–11807 (2007).
19. J. Hu, V. Tarasov, A. Agarwal, L. Kimerling, N. Carlie, L. Petit, and K. Richardson, "Fabrication and testing of planar chalcogenide waveguide integrated microfluidic sensor," *Opt. Express* **15**(5), 2307–2314 (2007).
20. U. Troitzsch and D. J. Ellis, "The ZrO<sub>2</sub>-TiO<sub>2</sub> phase diagram," *J. Mater. Sci.* **40**(17), 4571–4577 (2005).
21. L. Y. Zhu, G. Yu, X. Q. Wang, and D. Xu, "Preparation, phase transformation and microstructure of Zr<sub>x</sub>Ti<sub>1-x</sub>O<sub>2</sub> (x=0.1-0.9) fine fibers," *J. Non-Cryst. Solids* **355**(1), 68–71 (2009).
22. M. Bellotto, A. Caridi, E. Cereda, G. Gabetta, M. Scagliotti, and G. M. Braga Marcazzan, "Influence of the oxygen stoichiometry on the structural and optical properties of reactively evaporated ZrO<sub>x</sub> films," *Appl. Phys. Lett.* **63**(15), 2056–2058 (1993).
23. B. Prasai, B. Cai, M. K. Underwood, J. P. Lewis, and D. A. Drabold, "Properties of amorphous and crystalline titanium dioxide from first principles," *J. Mater. Sci.* **47**(21), 7515–7521 (2012).
24. S. Heiroth, R. Ghisleni, T. Lippert, J. Michler, and A. Wokaun, "Optical and mechanical properties of amorphous and crystalline yttria-stabilized zirconia thin films prepared by pulsed laser deposition," *Acta Mater.* **59**(6), 2330–2340 (2011).
25. B. Cho, J. Wang, L. Sha, and J. P. Chang, "Tuning the electrical properties of zirconium oxide thin films," *Appl. Phys. Lett.* **80**(6), 1052–1054 (2002).
26. Y. Gao, Y. Masuda, H. Ohta, and K. Koumoto, "Room-temperature preparation of ZrO<sub>2</sub> precursor thin film in an aqueous peroxozirconium-complex solution," *Chem. Mater.* **16**(13), 2615–2622 (2004).
27. R. H. French, S. J. Glass, F. S. Ohuchi, Y. N. Xu, and W. Y. Ching, "Experimental and theoretical determination of the electronic structure and optical properties of three phases of ZrO<sub>2</sub>," *Phys. Rev. B Condens. Matter* **49**(8), 5133–5142 (1994).
28. R. Swanepoel, "Determination of the thickness and optical constant of amorphous silicon," *J. Phys. E Sci. Instrum.* **16**(12), 1214–1222 (1983).
29. J. J. Yoon, S. M. Lee, T. J. Kim, S. Y. Hwang, M. Diware, Y. D. Kim, S. M. Hwang, and J. Joo, "Optical study of sol-gel processed ZrO<sub>2</sub>/Si films by spectroscopic ellipsometry," *J. Vac. Sci. Technol. B* **29**(4), 04D108 (2011).
30. R. Singh, M. Kumar, and S. Chandra, "Growth and characterization of high resistivity c-axis oriented ZnO films on different substrates by RF magnetron sputtering for MEMS applications," *J. Mater. Sci.* **42**(12), 4675–4683 (2007).
31. X. Zhao and D. Vanderbilt, "Phonons and lattice dielectric properties of zirconia," *Phys. Rev. B* **65**(7), 075105 (2002).
32. A. R. Pal, B. K. Sarma, N. C. Adhikary, J. Chutia, and H. Bailung, "TiO<sub>2</sub> polycrystalline nanocomposite films prepared by magnetron sputtering combined with plasma polymerization process," *Appl. Surf. Sci.* **258**(3), 1199–1205 (2011).
33. D. C. Cronemeyer, "Infrared absorption of reduced rutile TiO<sub>2</sub> single crystals," *Phys. Rev.* **113**(5), 1222–1226 (1959).

## 1. Introduction

Planar integrated MIR photonic devices constitute the basic device building block for MIR nonlinear optics, free-space optical communications, and spectroscopic sensing. Compared to their fiber counterparts, planar structures feature superior device robustness, and are amenable to high-volume production and integration with other on-chip components. In particular, planar optical resonators are capable of dramatically augment photon-matter interactions through optical resonance enhancement effects, thus making them ideal candidates for the aforementioned MIR applications. MIR resonators including micro-ring resonators [1–5], micro-disk resonators [6], and photonic crystal cavities [7,8] were demonstrated with high quality factors up to  $2.8 \times 10^5$ , which contribute to strong optical resonance enhancement. Optical materials highly transparent in the MIR range are required for these passive device fabrication. However, the widely adopted silicon-on-insulator (SOI) platform in near infrared is no longer suitable for MIR due to strong absorption of SiO<sub>2</sub> beyond 3.5 μm wavelength [3].

A variety of materials systems have been investigated in the past years, including suspended silicon [2], silicon on sapphire (SOA) [3], silicon on nitride [14], and chalcogenide glasses [6]. In this paper, we explore amorphous transition metal oxide thin films as a new material platform for MIR planar photonic device processing. Unlike silica, these oxides exhibit much lower phonon energy, which accounts for their broad optical transparency from visible extending into the MIR. The amorphous nature of these oxide films further enables monolithic deposition and fabrication on a wide variety of substrate materials, thus offering a significantly simplified processing alternative to single-crystalline wafer bonding and suspended structure release. The other competitive advantages of the oxides include: (1) superior thermal, mechanical and chemical stability (in particular, stability in oxidizing environments); (2) excellent biocompatibility; (3) low tendency of aging (i.e. sub- $T_g$  structural relaxation); (4) good surface affinity to biochemical functional groups containing oxygen; (5) large refractive index range (1.6 - 2.2 in the MIR) (6) proven compatibility with state-of-the-art CMOS technology as high-k dielectrics and ease of integration. (7) large optical nonlinearity (Kerr coefficient  $n_2 = 9.4 \times 10^{-15}$  [13] for  $\text{TiO}_2$  compared to  $2.5 \times 10^{-15}$  for  $\text{SiN}$  [15]) These notable features combined make transition metal oxides highly attractive materials for as planar MIR photonic devices.

So far, studies on transition metal oxides based planar photonic devices have exclusively focused on in visible and near infrared wavelengths. Waveguides with low propagation loss [9,11], and resonators [12] with high quality factors have been demonstrated using  $\text{TiO}_2$  or  $\text{ZrO}_2$  thin films. In single crystal Y doped  $\text{ZrO}_2$ , the material was demonstrated to be transparent in the wavelength range from 0.4  $\mu\text{m}$  to 6  $\mu\text{m}$  [10] with a relatively low refractive index of 1.98 at 5.2  $\mu\text{m}$ . For  $\text{TiO}_2$ , due to its lower optical band gap compared to  $\text{ZrO}_2$ , amorphous  $\text{TiO}_2$  film shows a high refractive index of about 2.2 in MIR [16]. In single crystal rutile  $\text{TiO}_2$ , lattice vibration induced multi-phonon absorption edge appears at shorter wavelengths of  $\sim 4.5 \mu\text{m}$  [17], limiting its applications for longer wavelength operation. A solid solution of  $\text{ZrO}_2\text{-TiO}_2$ , on the other hand, combines a relatively high index of refraction and low absorption loss up to 5  $\mu\text{m}$  wavelength, both are essential for compact, high quality factor on-chip MIR photonic resonators. Meanwhile, material crystallinity can also be tuned by Ti addition to decrease the scattering loss, making this system very attractive for MIR photonic device applications.

To the best of our knowledge, there has been no report on mid-infrared photonic devices based on transition metal oxides in the system of  $\text{ZrO}_2\text{-TiO}_2$ . In this report, we systematically studied the  $\text{ZrO}_2\text{-TiO}_2$  (ZTO) thin film material structure and optical properties as a function of Ti concentration. Amorphous, smooth and low loss ZTO thin films were prepared with a Ti concentration of 40 at.%. We also fabricated and tested micro-disk resonators using  $\text{Ge}_{23}\text{Sb}_7\text{S}_{70}/\text{Zr}_{0.6}\text{Ti}_{0.4}\text{O}_2$  strip-loaded structures at 5.2  $\mu\text{m}$  MIR wavelength. We demonstrate that  $\text{ZrO}_2\text{-TiO}_2$  thin films are promising material candidates for on-chip MIR photonic devices.

## 2. Experiments

ZTO thin films were deposited by radio-frequency (RF) reactive magnetron sputtering. A 4 inch Zr-Ti metal (purity 99.95%) composite target was used. A Zr metal target was uniformly cut into 16 sectors with a sector angle of  $22.5^\circ$ , by replacing 0, 1, 2, 4, 8 sectors with Ti metal sectors with identical sizes, Ti areal fraction of 0%, 6.25%, 12.5%, 25% and 50% can be achieved on the target. Ar and  $\text{O}_2$  mixture (> 99.999% purity) with a flow rate ratio of  $\text{Ar}:\text{O}_2 = 9:1$  was used as the sputtering ambient gas. The deposition pressure was kept at 3.75 mTorr, and the sputtering power was fixed at 400 W, leading to a deposition rate of 2 - 3 nm/min, which increases with Ti concentration. Several types of substrates were used for film deposition, including double side polished silicon wafers, glass slides and MIR-transparent MgO substrates. There is no clear phase and structural difference between thin films on different substrates. All depositions were carried out at room temperature. The substrates

were attached to a water cooled sample holding stage to maintain the substrates at relatively low temperature during deposition. Transparent, colorless or slightly pink colored thin films with various Ti concentrations were obtained after deposition with film thickness ranging from 250 nm to 360 nm measured by cross-sectional SEM.

Phase identification and crystal structure analysis were carried out using X-ray diffraction (XRD) on a Shimadzu XRD-7000 X-ray diffractometer operating in a standard  $\omega$ - $2\theta$  scan mode. Film morphology and thickness were characterized by a JEOL7600F field emission scanning electron microscopy (SEM). Atomic concentrations of Zr and Ti were analyzed using energy dispersive spectroscopy (EDS) on SEM. The resulting films show Ti concentrations of 4 at.%, 10 at.%, 20 at.% and 40 at.% on the Zr site in the ZTO films. Optical transmittance of thin films on glass substrates were measured using a Perkin-Elmer LAMBDA 750 UV/VIS/NIR spectrometer with an integrating sphere in the wavelength range from 200 nm to 2500 nm. Transmittance spectra were also collected on several films grown up to 500 nm on glass slides for film index determination. To quantify mid-infrared phonon vibration modes in the oxides, reflectance spectra of the films were measured using Fourier transformed infrared spectroscopy (FTIR) on a Bruker Tensor27 FTIR spectrometer with an A562 mid-infrared integrating sphere at room temperature.

The waveguides and resonators were defined using lift-off patterning [18]. In the fabrication process, a layer of NR9-3000PY resist (Futurex Inc.) was first spin-coated onto the  $Zr_{0.6}Ti_{0.4}O_2$  film, followed by UV exposure carried out on a Karl Suss aligner and development to pattern the resist layer. The bulk GeSbS glass powders was then thermally deposited onto the  $Zr_{0.6}Ti_{0.4}O_2$  film in a custom-designed thermal evaporator (PVD Products Inc.) [19]. The film was deposited at a base pressure of  $2 \times 10^{-7}$  Torr using a Tantalum baffled source, and the deposition rate was stabilized at 20 Å/s. The MgO substrate was mounted on a thermostat stage and was maintained at room temperature throughout the deposition process. In the last step, the sample was sonicated in acetone to dissolve the photoresist layer beneath the undesired parts of the  $Ge_{23}Sb_7S_{70}$  film, thus lifting it off to create the waveguide patterns. Optical transmission characterization is carried out on a MIR fiber end coupled system to the resonator device, detailed description of the characterization process is described in [6].

### 3. Results and discussion

Figure 1 shows the  $\omega$ - $2\theta$  scan XRD spectrum of ZTO films on Si(001) substrates with various Ti concentrations, also shown are the *pseudo-cubic* lattice constant and grain size as a function of Ti concentration. For pure  $ZrO_2$ , the film is polycrystalline with a predominantly monoclinic phase and a small amount of tetragonal phase. The mixture of tetragonal and monoclinic  $ZrO_2$  phases was observed in previous reports as well [20], which was shown to be strongly dependent on oxygen partial pressure during deposition. With increasing Ti concentration up to 20 at.%, the tetragonal phase disappears and the thin films remain monoclinic, indicating a solid solution based on  $ZrO_2$  monoclinic lattice. When Ti concentration reaches 40 at.%, the film becomes amorphous with a broad characteristic diffraction pattern, suggesting that the critical concentration for growing an amorphous ZTO film is between 20 at.% to 40 at.% of Ti concentration. It is worth noting that the high solubility of Ti in the monoclinic  $ZrO_2$  phase was not identified in the phase diagram [16]. Such single-phase solution compounds were also observed in sol-gel prepared crystal fibers [17].

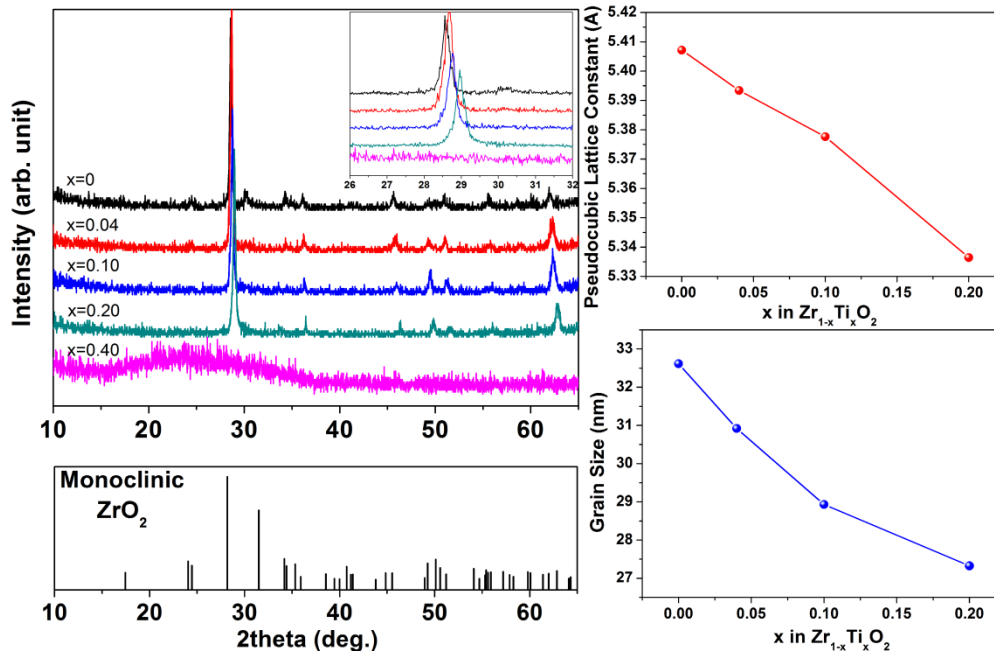


Fig. 1. XRD of ZTO thin films with different Ti concentrations. Amorphous ZTO thin film is achieved in  $Zr_{0.6}Ti_{0.4}O_2$ . Also shown are the pseudocubic lattice constant and grain size as a function of Ti concentration

We calculated the lattice constants by assuming a *pseudo-cubic* unit cell of the crystals, using the ZTO(11 $\bar{1}$ ) diffraction peak at around  $2\theta = 28^\circ$ . Due to the smaller ionic radius of  $Ti^{4+}$  compared to  $Zr^{4+}$ , the lattice constant monotonically decreases with Ti doping, consistent with previous observations [21]. Crystal size of the ZTO thin films is calculated by applying the Scherrer equation to the ZTO(11 $\bar{1}$ ) diffraction peak. The crystal size is around 30 nm and decreases with Ti doping, suggesting that the material becomes increasingly difficult to crystallize with progressive Ti addition.

Figure 2(a) shows the optical transmittance of ZTO thin films on glass substrates in the ultraviolet to near infrared wavelength range. All the films show high optical transparency above 400 nm. The intensity noise at 300~350 nm wavelength range was caused by environmental light. Clear optical interference patterns were observed. Optical band gap of ZTO films were estimated from the material absorption edge using a Tauc-plot [24]. With increasing Ti concentration, the thin film optical band gap decreases from 4.34 eV to 4.11 eV. Note that the optical band gap shows almost a linear relationship with Ti doping at concentrations lower than 20 at.%. This behavior (the Vegard's law) is consistent with the substitutional solid solution structure of ZTO measured by XRD; whereas amorphous  $Zr_{0.6}Ti_{0.4}O_2$  clearly deviates from this line with a wider optical band gap. Such band gap increase was also observed in amorphous  $TiO_2$  [23] and yttrium stabilized  $ZrO_2$  (YSZ) [24] compared to their crystalline counterparts. Compared to the literature reported  $ZrO_2$  optical band gap value of 4.6 - 7.8 eV [25], our films show a relatively small optical band gap. Similar results were also observed in solution deposited or sputter deposited  $ZrO_2$  thin films [26], which may be explained by the partially amorphous film structure or structural disorder in the  $ZrO_2$  thin films [27]. The index of refraction of ZTO films is extracted using the Swanepoel method [28] and the Cauchy's equation  $n(\lambda) = B + C/\lambda^2$ , where the maxima (TM) and minima (Tm) of transmittance are fitted using a cubic spline interpolation, and the material index was calculated using the interpolated values. Due to the few interference

fringes at longer wavelengths in  $Zr_{0.9}Ti_{0.1}O_2$  and  $Zr_{0.6}Ti_{0.4}O_2$  films, the refractive index is fitted only up to 1000 nm wavelength. It is obvious that increasing Ti concentration results in increased thin film index in the near infrared wavelength range. It is also worth noting that the  $ZrO_2$  index of refraction agrees with literature reports [29], which further corroborates the fitting results using this method.

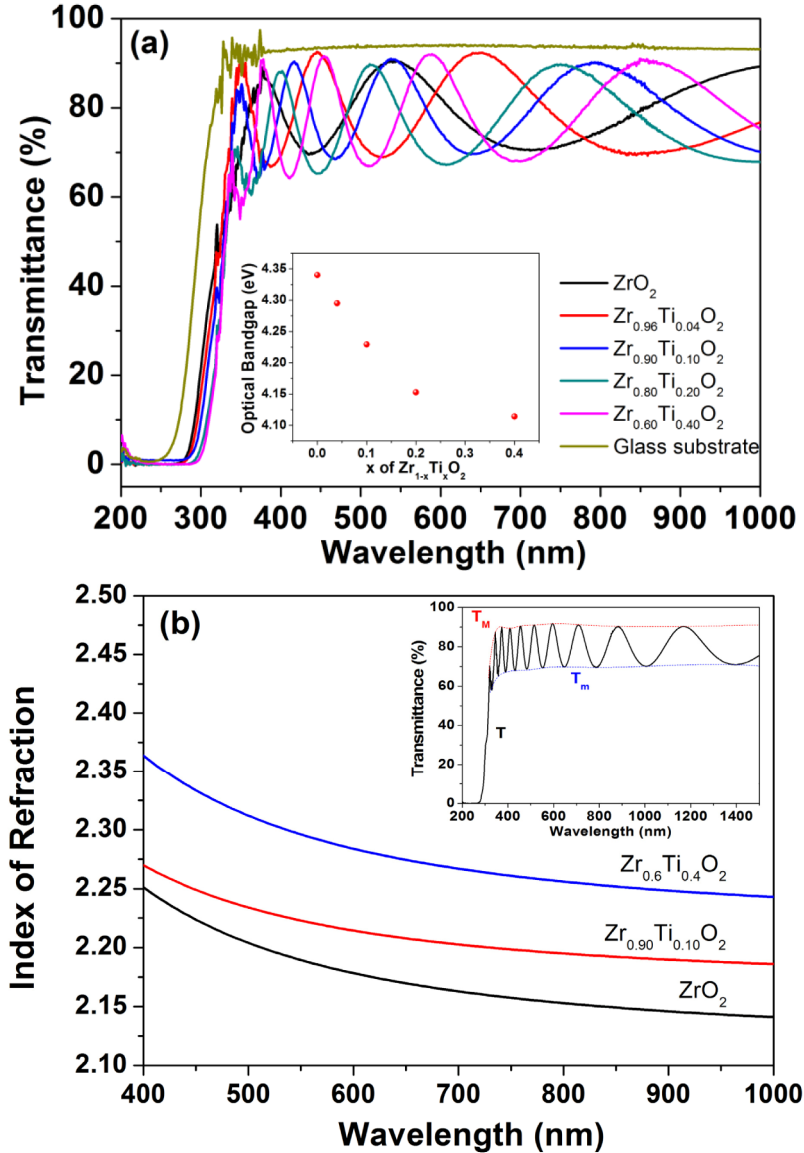


Fig. 2. (a) UV-VIS-NIR transmission spectrum of ZTO films with various Ti concentrations. The inset shows the optical bandgaps of ZTO thin films. (b) Refractive index of ZTO thin films with 3 Ti concentrations in the visible to near infrared wavelength range, calculated following reference [28]

In order to understand the phonon vibration modes of ZTO films in the infrared, FTIR spectroscopy measurement was carried out on thin films on silicon substrates. We focus on the frequency range of  $400\text{ cm}^{-1}$  to  $1000\text{ cm}^{-1}$  where the phonon vibration modes exist for  $TiO_2$  and  $ZrO_2$ . The absorption peak appearing at  $600\text{ cm}^{-1}$  for all samples is from the silicon

substrate [30]. For the  $\text{ZrO}_2$  film, two characteristic phonon vibration absorption peaks are observed at around  $560\text{ cm}^{-1}$  and  $480\text{ cm}^{-1}$ , respectively, which agrees very well with first-principle calculation results of  $483\text{ cm}^{-1}$  and  $571\text{ cm}^{-1}$  for monoclinic  $\text{ZrO}_2$  [31]. There is no obvious shift of these phonon modes with increasing Ti concentration up to 20 at.%, whereas the reflection spectrum becomes broadened with Ti incorporation with less features of the absorption peaks. This can be explained by an overlay of the Ti-O broad absorption band in the  $400\text{ cm}^{-1}$  to  $1800\text{ cm}^{-1}$  frequency range [32] with Zr-O vibration modes. In  $\text{Zr}_{0.6}\text{Ti}_{0.4}\text{O}_2$ , no clear Zr-O phonon absorption peaks can be observed and the thin film becomes broadband absorptive in the  $400\text{ cm}^{-1}$  to  $1000\text{ cm}^{-1}$  range, which is consistent with the high Ti concentration and amorphous structure of the thin film.

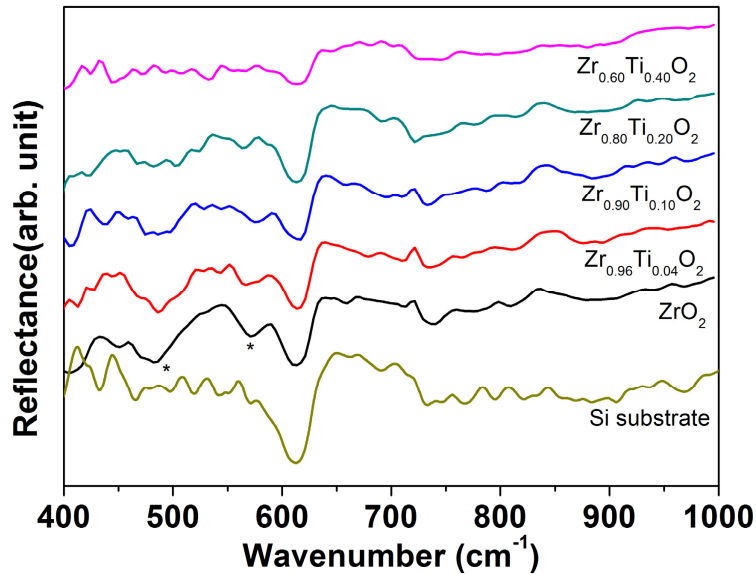


Fig. 3. FTIR of silicon substrate and ZTO thin films on silicon with different Ti concentrations. \* indicates the major phonon vibration modes of Zr-O in the infrared wavelength range.

Optical transparency of the  $\text{Zr}_{0.6}\text{Ti}_{0.4}\text{O}_2$  film at the  $5.2\text{ }\mu\text{m}$  mid-infrared wavelength was experimentally validated using planar optical resonator measurements. Planar waveguiding devices (waveguides and micro-disk resonators) were fabricated by patterning a layer of  $\text{Ge}_{23}\text{Sb}_7\text{S}_{70}$  chalcogenide glass on top of the  $\text{Zr}_{0.6}\text{Ti}_{0.4}\text{O}_2$  film to form strip-loaded structures (Figs. 4(a) and 4(b)). Figure 4(c) shows an SEM cross-sectional image of the fabricated strip-loaded waveguide. We chose  $\text{Ge}_{23}\text{Sb}_7\text{S}_{70}$  glass as the strip-loading material given its known mid-IR transparency [6]. Field intensity distribution of the quasi-TE polarized optical mode at  $5.2\text{ }\mu\text{m}$  wavelength is illustrated in Fig. 4(d), showing strong modal field overlap with the  $\text{Zr}_{0.6}\text{Ti}_{0.4}\text{O}_2$  film with a confinement factor of 22% in the oxide layer.

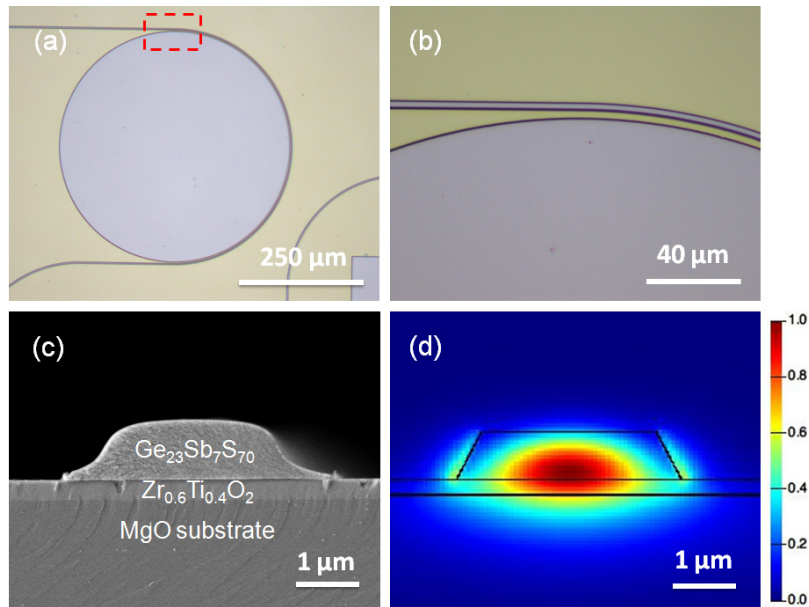


Fig. 4. (a, b) Top-view optical micrographs of micro-disk resonators comprising a  $\text{Ge}_{23}\text{Sb}_7\text{S}_{70}$ - $\text{Zr}_{0.6}\text{Ti}_{0.4}\text{O}_2$  strip-loaded structure; the coupling gap region (the red box in Fig. a) between the micro-disk and the bus waveguide is shown in Fig. b; (c) cross-sectional SEM image of a mid-IR waveguide illustrating the strip-loading structure; (d) field intensity distribution of the quasi-TE polarized waveguide mode simulated using FDTD.

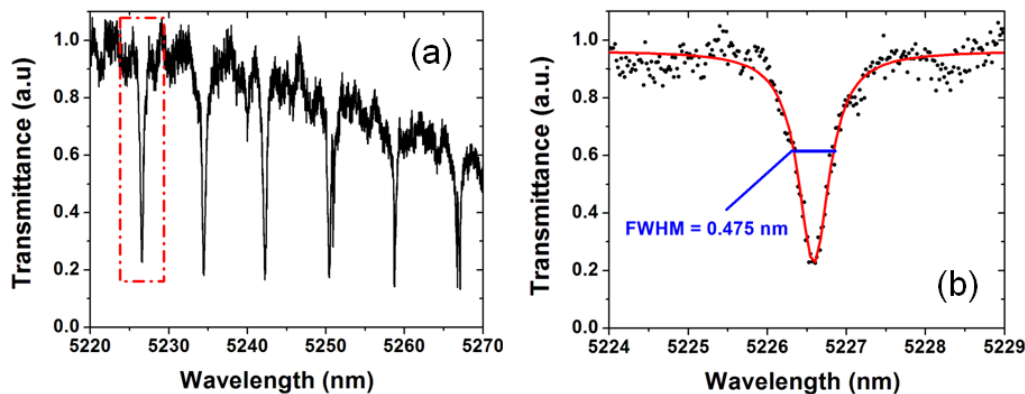


Fig. 5. Transmission spectra of the  $\text{Ge}_{23}\text{Sb}_7\text{S}_{70}$ - $\text{Zr}_{0.6}\text{Ti}_{0.4}\text{O}_2$  mid-IR resonators: Fig. b shows the spectrum in the red box in Fig. a.

Transmission spectra through the strip-loaded micro-resonators were measured using an external cavity tunable quantum cascade laser near the  $5.2\ \mu\text{m}$  wave band. The laser light was launched into the bus waveguides via fiber end-fire coupling following protocols outlined in a previous publication [6]. Figure 5 plots the transmittance spectra through a bus waveguide. The loaded cavity quality factor (Q-factor) was fitted from the resonant peak full width at half maximum (FWHM) to be approximately 11,000 (Fig. 4(b)), which corresponds to an equivalent waveguide loss of  $(8.8 \pm 1.4)$  dB/cm. Optical loss measurement performed on reference devices made of  $\text{Ge}_{23}\text{Sb}_7\text{S}_{70}$  chalcogenide glass and of identical dimensions yielded a loss value of  $(6.3 \pm 1.5)$  dB/cm. Compared to the waveguide loss in ref. 6, we consider the MgO substrate is the main source of optical loss in our devices. As a conservative estimation, assuming all the excess loss of  $(2.5 \pm 2.1)$  dB/cm is caused by the ZTO film and considering the 22% optical confinement factor in the ZTO film, the result indicates an upper limit of  $\sim 10$

dB/cm material attenuation in ZTO at 5.2  $\mu\text{m}$  wavelength, although the large error bar suggests that the actual ZTO material loss may be well below 10 dB/cm. From the loss values of single crystal  $\text{ZrO}_2$  and  $\text{TiO}_2$  [11, 33], we can expect a low loss level of about 2 dB/cm in the ZTO films at 5.2  $\mu\text{m}$  wavelength. Further investigation is required to more accurately quantify and improve the material loss. Nevertheless, the high quality factor resonator indicates ZTO can serve as a promising material for planar MIR photonic devices. Microfabrication of a ZTO/MgO ridge waveguide is under development to further improve the device performance and for sensing applications.

#### 4. Conclusions

In conclusion,  $(\text{ZrO}_2)_x(\text{TiO}_2)_{1-x}$  thin films with  $x$  ranging from 0 to 0.4 were deposited by reactive sputtering. The thin film material structure and optical properties were systematically studied as a function of Ti concentration. Transparent, amorphous and high index  $\text{Zr}_{0.6}\text{Ti}_{0.4}\text{O}_2$  films were prepared by low temperature deposition on MgO substrates. We further demonstrated micro-disk resonators consisting of  $\text{GeS}_2/\text{Zr}_{0.6}\text{Ti}_{0.4}\text{O}_2$  strip-loaded structures with a loaded quality factor of 11,000 at 5.2  $\mu\text{m}$  MIR wavelength. The low optical loss of ZTO thin films indicates their potential for integrated MIR photonic device fabrication.

#### Acknowledgment

This work is supported by the University of Electronic Science and Technology of China (Grant No. A1098531023601024). H. Lin, L. Li and J. Hu acknowledge partial funding support provided by NSF under award number 1200406. The authors cordially thank S. Danto and K. Richardson for supplying the  $\text{Ge}_{23}\text{Sb}_7\text{S}_{70}$  bulk glass for device fabrication.